CrossMark

MOSEL Survey: JWST Reveals Major Mergers/strong Interactions Drive the Extreme Emission Lines in the Early Universe

Anshu Gupta[1,2] , Ravi Jaiswar[1,2] , Vicente Rodriguez-Gomez[3,4] , Ben Forrest[5] , Kim-Vy Tran[2,6,7] ,
Themiya Nanayakkara[2,8] , Anishya Harshan[9] , Elisabete da Cunha[2,10] , Glenn G. Kacprzak[2,11] , and
Michaela Hirschmann[12,13]

[1] International Centre for Radio Astronomy Research (ICRAR), Curtin University, Bentley, WA, Australia
[2] ARC Centre of Excellence for All Sky Astrophysics in 3 Dimensions (ASTRO 3D), Australia
[3] Department of Physics and Astronomy, Johns Hopkins University, Baltimore, MD 21218, USA
[4] Instituto de Radioastronomía y Astrofísica, Universidad Nacional Autónoma de México, A.P. 72-3, 58089 Morelia, Mexico
[5] Department of Physics and Astronomy, University of California Davis, One Shields Avenue, Davis, CA, 95616, USA
[6] School of Physics, University of New South Wales, Sydney, NSW 2052, Australia
[7] Center for Astrophysics | Harvard & Smithsonian, Cambridge, MA, USA
[8] Centre for Astrophysics and Supercomputing, Swinburne University of Technology, Hawthorn, VIC 3122, Australia
[9] University of Ljubljana, Department of Mathematics and Physics, Jadranska ulica 19, SI-1000 Ljubljana, Slovenia
[10] International Centre for Radio Astronomy Research, University of Western Australia, 35 Stirling Highway, Crawley, WA 6009, Australia
[11] Swinburne University of Technology, Hawthorn, VIC 3122, Australia
[12] Institute of Physics, GalSpec, Ecole Polytechnique Federale de Lausanne, Observatoire de Sauverny, Chemin Pegasi 51, 1290 Versoix, Switzerland
[13] INAF, Astronomical Observatory of Trieste, Via Tiepolo 11, I-34131 Trieste, Italy

Abstract

Extreme emission line galaxies (EELGs), where nebular emissions contribute 30%–40% of the flux in certain photometric bands, are ubiquitous in the early Universe ($z > 6$). We utilize deep NIRCam imaging from the JWST Advanced Deep Extragalactic Survey (JADES) to investigate the properties of companion galaxies (projected distance <40 kpc, $|dv| < 10{,}000$ km s^{-1}) around EELGs at $z \sim 3$. Tests with TNG100 simulation reveal that nearly all galaxies at $z = 3$ will merge with at least one companion galaxy selected using similar parameters by $z = 0$. The median mass ratio of the most massive companion and the total mass ratio of all companions around EELGs is more than 10 times higher the control sample. Even after comparing with a stellar mass and stellar mass plus specific star formation rate (SFR)-matched control sample, EELGs have 3 to 5 times higher mass ratios than the brightest companion and total mass ratio of all companions. Our measurements suggest that EELGs are more likely to be experiencing strong interactions or undergoing major mergers irrespective of their stellar mass or specific SFRs. We suspect that gas cooling induced by strong interactions and/or major mergers could be triggering the extreme emission lines, and the increased merger rate might be responsible for the overabundance of EELGs at $z > 6$.

1. Introduction

In the past decade, deep photometric surveys with Spitzer and Hubble Space Telescope (HST) revealed more than two orders increase in the [O III] 5007+Hβ equivalent width (EW) of galaxies between $z = 0$ and 6 (Labbé et al. 2013; Roberts-Borsani et al. 2016; Barro et al. 2019; Mainali et al. 2019; Endsley et al. 2020; Gupta et al. 2022). Direct observations with the James Webb Space Telescope (JWST) in the past year have confirmed that 80% of galaxies have [O III] 5007+Hβ EW >800 Å; almost 3 times the EW of a typical star-forming galaxy at $z \sim 2$ (Cameron et al. 2023; Endsley et al. 2023; Rinaldi et al. 2023; Tang et al. 2023). Thus, understanding the physical origin of extreme emission lines is becoming increasingly important to understand the early galaxy evolution.

Extreme emission line galaxies (EELGs) at lower redshifts typically have low stellar masses and high star formation rates (Atek et al. 2011; van der Wel et al. 2011; Maseda et al. 2013, 2014; Chevallard et al. 2018; Tang et al. 2019;

Gupta et al. 2022; Lumbreras-Calle et al. 2022) and might be undergoing the first burst in their star formation history (Cohn et al. 2018; Endsley et al. 2023). Reddy et al. (2018) show that evolution of stellar mass and star formation main sequence is sufficient to explain the moderate increase in the [O III] 5007 EW between $z = 0$ and $z \sim 2$. Although, it is possible that increased stochasticity in the star formation history is sufficient to explain the overabundance of EELGs in the early Universe (Dressler et al. 2023; Endsley et al. 2023).

Mergers of gas-rich galaxies and galaxy–galaxy interactions can funnel gas into the galactic center, boosting the star formation (Sanders & Mirabel 1996; Hayward et al. 2013; Sparre & Springel 2017; Moreno et al. 2019). Cosmological zoom-in simulations show that scatter in the star-forming main sequence is due to mergers and gas accretion events (Tacchella et al. 2016; Sparre et al. 2017; Torrey et al. 2018), and the gas accretion events also set the intermediate-scale (<1 Gyr) variability in the star formation history (Sparre et al. 2017; Tacchella et al. 2020). Mergers and galaxy–galaxy interaction can induce the circumgalactic medium gas to cool down, boosting the star formation rate by 30%–40% (Moreno et al. 2019; Sparre et al. 2022).

Traditionally, asymmetry and smoothness in the stellar light profile of galaxies are used to identify galaxies undergoing
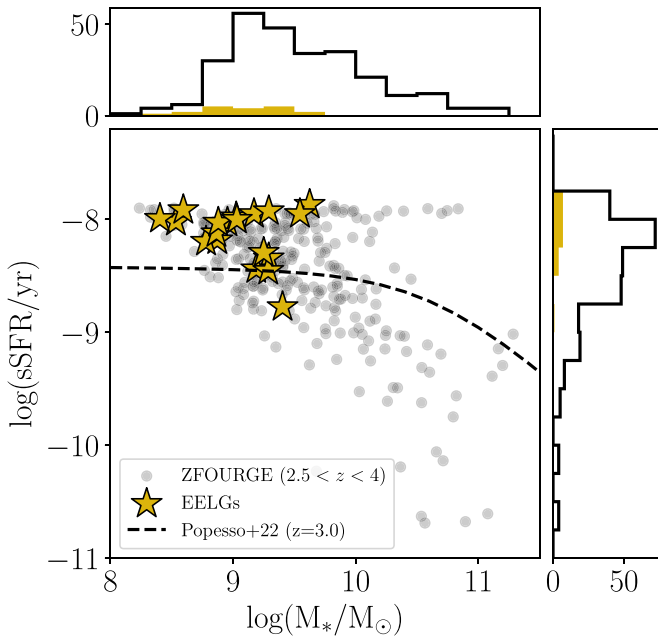
Figure 1. Stellar mass and specific SFR distribution of EELGs (golden stars) and full control sample (gray circles). The SFR are derived from the MAGPHYS SED fitting code. The dashed line corresponds to the star-forming main sequence at $z = 3$ by Popesso et al. (2022). At a fixed stellar mass EELGs have 0.3 dex higher sSFR compared to the control galaxies.

major mergers (Conselice 2003; Lotz et al. 2004). However, mock imaging of simulated galaxies shows that the accuracy of morphology indicators varies between 30% and 60% and depends significantly on the choice of photometric filter (Rose et al. 2023). Sophisticated photometric and/or deep spectroscopic observations have been used to identify pairs of galaxies that would end up merging together at some point (Lin et al. 2004; Duncan et al. 2019; Watson et al. 2019).

In this Letter, we use the deep NIRCam photometry from the JWST Advanced Deep Extragalactic Survey (JADES; Bunker et al. 2023; Eisenstein et al. 2023; Hainline et al. 2023; Rieke & the JADES Collaboration 2023) to analyze the properties of companions around EELGs at $z \sim 3$. The EELGs were identified in the FourStar Galaxy Evolution Survey (ZFOURGE; Straatman et al. 2016) using composite spectral energy distribution (SED) fitting (Forrest et al. 2018) and later confirmed as part of the Multi-Object Spectroscopic of Emission Line (MOSEL) survey (Tran et al. 2020; Gupta et al. 2022). We find that EELGs are more likely to have similar stellar mass companions than the control sample, suggesting they are more likely to be either undergoing major mergers or experiencing strong interactions.

2. Data

The EELG sample is selected from ZFOURGE (Straatman et al. 2016), which uses medium-band filters in the J and H bands on the FourStar instrument ($13' \times 13'$) on the Magellan telescope to reach a photometric redshift accuracy of $<2\%$ at $1.5 < z < 4$ (Nanayakkara et al. 2016; Tran et al. 2020). Forrest et al. (2018) identified 76 EELGs between $2.5 < z < 4$ in the Chandra Deep Field South (CDFS) using a composite SED fitting. For comparison, we also select 1712 galaxies within the same redshift range and K-band signal-to-noise ratio (S/N) > 10 from the ZFOURGE survey.

The first data release (DR1) of JADES presents unprecedented depth (4.5 nJy at 5σ in F444W) for ~ 25 arcmin^2 (Bunker et al. 2023; Eisenstein et al. 2023; Hainline et al. 2023; Rieke & the JADES Collaboration 2023) within the CDFS (Rieke et al. 2023; Williams et al. 2023). We match the brightest galaxy in the F444W filter within $0''5$ to crossmatch ZFOURGE and JADES samples, to account for small astrometric offset ($\sim 0''3$) between the two surveys. We find only 19 out of 76 EELGs and 275 out of 1712 control galaxies in the JADES DR1 because of its relatively smaller footprint compared to the ZFOURGE survey.

3. Analysis

3.1. Photometric Redshifts

To identify companion galaxies, we need redshifts for EELGs, the control sample, and their possible companions. Only 12/19 [66/275] of EELGs [control] have spectroscopic redshifts either from the MOSEL survey (Tran et al. 2020; Gupta et al. 2022) or JADES DR1, which has collected spectroscopic redshifts from many surveys in the literature plus the FRESCO survey (Oesch et al. 2023) and NIRSpec observation by JADES (Rieke & the JADES Collaboration 2023).

Both ZFOURGE and JADES surveys use EAZY (Brammer et al. 2008) to calculate photometric redshifts. Additional stellar templates with younger stellar ages were added by the JADES team (Hainline et al. 2023). We do not find any systematic difference in the photometric redshifts from JADES and ZFOURGE surveys. The average offset between the photometric redshift and spectroscopic redshift for EELGs [control] is $<z_{spec} - z_{phot}> = -0.09$ [−0.01], $\sigma_{NMAD} = 0.017$ [0.019], and zero outliers [3%] from the JADES survey. For consistency, we use photometric redshifts from the JADES DR1 throughout this Letter when spectroscopic redshifts are unavailable.

3.2. Spectral Energy Distribution

We use the MAGPHYS (da Cunha et al. 2008, 2015) SED fitting code with the BC03 stellar population synthesis model (Bruzual & Charlot 2003), delayed exponentially declining star formation history model, and Charlot & Fall (2000) dust attenuation law to derive physical properties. The results presented in this Letter were derived only using the 23-band photometry from the JADES DR1 (HST + broadband JADES + JWST Extragalactic Medium-band Survey, JEMS; Williams et al. 2023) and fixing the redshift to the best redshift determined in Section 3.1 because most companions are undetected in ZFOURGE.

Figure 1 shows the stellar mass and specific star formation rate (sSFR) distribution of our primary targets. As expected EELGs have higher sSFRs and lower stellar mass than the control sample by about 0.3 dex (Table 1; Forrest et al. 2018; Gupta et al. 2022). MAGPHYS does not include emission lines, the exclusion of which can increase the estimated stellar masses by up to 0.5 dex, especially for EELGs (Forrest et al. 2018). However, our stellar masses do not change significantly (<0.04 dex) after removing filters (F277W or F277W plus F356W) that will be contaminated with [O III] 5007 and Hα emission lines. We suspect the inclusion of longer-wavelength filters (F356W and F444W) and their broadness minimize the effect of emission lines on stellar mass estimates.
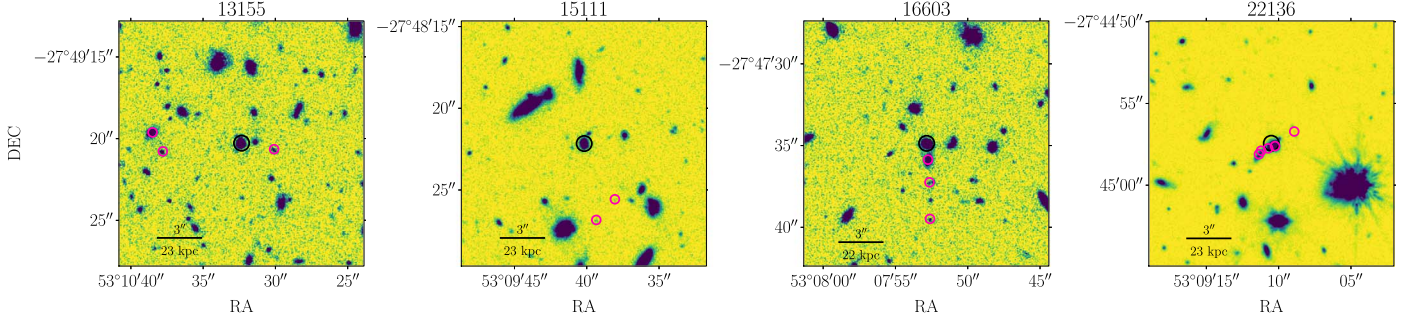
Figure 2. Example JWST/NIRCam F444W images from the JADES survey (Rieke & the JADES Collaboration 2023) for four EELGs (black circles and their companions (pink circles) showing the variety of companions around the target galaxy.

Table 1
Properties of Companions

Sample	N_c [a,b]	$\max(M_{*,c})/M_{*,t}$ [a,c]	$\Sigma M_{*,c}/M_{*,t}$ [a,d]
EELGS	2^{+1}_{-0}	$0.65^{+0.11}_{-0.51}$	$0.71^{+0.27}_{-0.34}$
ZFOURGE ($2.5 < z < 4$)	1^{+1}_{-0}	$0.05^{+0.05}_{-0.02}$	$0.07^{+0.04}_{-0.04}$
M_*-matched	1^{+1}_{-0}	$0.15^{+0.12}_{-0.03}$	$0.20^{+0.17}_{-0.08}$
M_*-sSFR-matched	1^{+1}_{-0}	$0.17^{+0.08}_{-0.07}$	$0.22^{+0.12}_{-0.08}$

Notes.
[a] Numbers represent the 50th, 16th, and 84th percentile errors.
[b] N_c is the number of companions.
[c] $\max(M_{*,c})/M_{*,t}$ is the stellar mass of the most massive companion to the target galaxy.
[d] $\Sigma M_{*,c}/M_{*,t}$ is the total stellar mass of all companions to the target galaxy.

3.3. Companion Galaxies

We use the distribution of galaxies in phase space to identify companions around the target galaxies. Spectroscopic studies of pair fraction measurements typically employ projected distances of 20–50 kpc and velocity offsets of $|dv| < 500$ km s^{-1} to identify interacting pairs of galaxies (Patton et al. 2000; Mantha et al. 2018). Studies relying on photometric redshifts adopt a more statistical approach to account for the uncertainty in photometric redshift measurements (López-Sanjuan et al. 2015; Duncan et al. 2019; Watson et al. 2019).

The companion analysis is restricted to all galaxies detected at S/N > 5 in the F444W filter. The choice of the F444W filter ensures that companion galaxies are well detected in all shorter-wavelength filters, which is necessary for accurate SED modeling and photometric redshift estimation. Only 4% of the galaxies with S/N > 5 in the F444W filter have spectroscopic redshifts and less than 10% have counterpart in ZFOURGE. Thus, we use the photometric redshifts provided by JADES DR1 for all samples when spectroscopic redshifts are unavailable. We estimate an average offset of $\langle z_{spec} - z_{phot}\rangle = 0.03$ and $\sigma_{NMAD} = 0.024$ with about a 13% catastrophic outlier. A slightly higher outlier fraction for our companion sample is because of the confusion between Lyman break and Balmer break at $z \sim 3$.

The results presented in this Letter use a projected distance $d_{pro} < 40$ kpc and velocity offset $|dv| < 10000$ km s^{-1} ($\sim 1.5 \times \sigma_{NMAD}$ companions). Figure 2 shows examples of companions identified around a subset of EELGs (See Table 2 in the Appendix). The primary conclusions of this Letter do not change significantly if we vary the maximum d_{pro} between 20 and 50 kpc and maximum $|dv|$ between 5000 and 20,000 km s^{-1}. Accuracy of photometric redshifts will strongly affect the properties of

companions identified in this Letter. About 75% [61%] of companions to EELGs [control] have $I > 0.75$, where I corresponds to the peakiness of the redshift probability distribution defined as $I = \int_{z_{peak}-\Delta z}^{z_{peak}+\Delta z} P(z)\,dz$, where $\Delta z = 0.1*(1+z_{peak})$. Our main conclusions do not change significantly if we restrict the analysis to companions with $I > 0.75$.

Unfortunately, we do not have a statistically significant number of spectroscopically confirmed EELGs or control galaxy pairs to test the companion identification technique (three true spectroscopic pairs out of four photometrically identified companions). We instead use cosmological simulations to quantify the accuracy of the companion identification technique (see Section 3.5).

The median number of companions around EELGs is two, whereas galaxies in the control sample only have one companion (Figure 3). About 16% of the EELGs (3 of 19) do not have any companion as apposed to 24% in the control sample. However, a standard two-sided Kolmogorov–Smirnov (KS) test suggests no significant difference between the distribution of number of companions around EELGs and the control sample. For EELGs, we find a weak negative correlation between the sSFR and the nearest neighbor distance (Spearman's coefficient ~ -0.6, with p-value $= 0.008$) but not for the control sample. We suspect that limited sample size and uncertainty in photometric redshift washes out this weak correlation.

To determine whether the galaxies are experiencing strong or weak interactions, we calculate the ratio of the stellar mass of the most massive companion and the total stellar mass of all companions to the target galaxy (Figure 4). For galaxies without a detected companion, we assign a maximum companion mass of $10^7 M_\odot$ (minimum stellar mass estimated for the full companion population). The median stellar mass ratio of the most massive companion to EELGs is ~ 0.65, whereas it is only 0.04 for the control (two-sided KS test $p = 0.007$) sample. The median stellar mass ratio of all companions combined is also less than 0.10 for the control sample ($p = 0.006$).

We use bootstrapping to account for the differences in the sample size, stellar mass, and sSFR distribution of the EELGs and control sample. For each bootstrapped iteration and sample, we randomly select 19 galaxies (equal to the total number of EELGs) while allowing for repeats. The stellar mass matching is done by randomly selecting one control galaxy for every EELG whose stellar mass is within 0.1 dex of the EELG (Kaasinen et al. 2016; Gupta et al. 2021). An additional restriction on sSFR to be within 0.1 dex of the EELG is
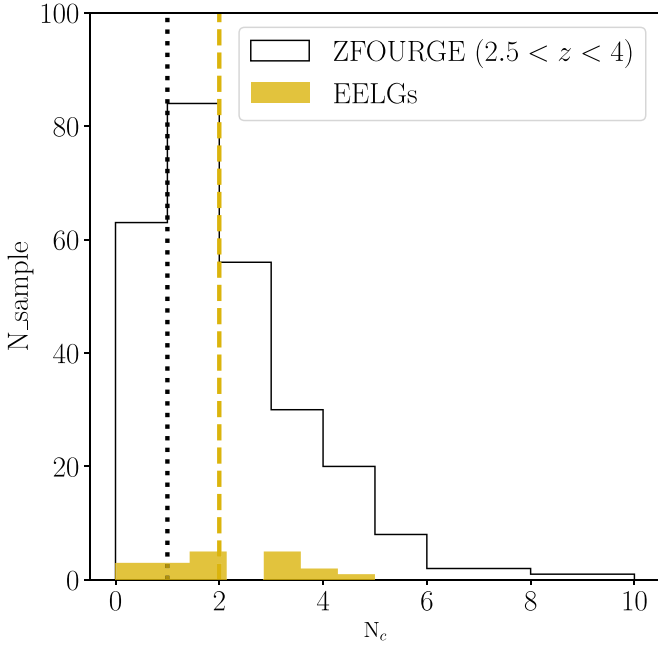
Figure 3. Distribution of the number of companions around EELGs (solid gold) and the control sample (black). The dashed lines indicate the medians of the respective samples. EELGs on average have two companions, whereas galaxies in the control sample only have one companion.

imposed for the stellar mass plus sSFR–matched control sample. We estimate a KS test $p > 0.4$ between EELG and the respective property of the matched samples for all iterations.

On average EELGs have two companion galaxies, and the stellar mass ratio of the most massive companion is 0.65 times the EELG (Figure 5). In contrast, the median mass ratio of the most massive companion and the total mass of all companions remains less than 0.34 and 0.37, respectively, for 90% of the iterations (Figure 5) across all control samples. Even compared to the stellar mass plus sSFR–matched sample, EELGs have 3 times more massive companions (Table 1). Thus, our measurements suggest that EELGs are more likely to be surrounded by similar stellar mass companions, and thus are more likely to be undergoing major mergers/experiencing strong interactions.

3.4. False Companion Contamination

False projections could result in a higher fraction of companions being identified per galaxy. To estimate this effect, we randomly positioned both EELGs and control galaxies at 1000 different locations and reidentified companions at each location, following the criteria outlined in the previous section (projected distance $d_{proj} < 40$ kpc and relative velocity $|dv| < 10{,}000$ km s^{-1}). We detected at least one companion at approximately 30% of the randomly chosen locations for both EELGs and control galaxies. The increased sensitivity of the JADES survey (4.5 nJy at 5σ), leads to a significantly higher contamination fraction compared to previous studies (Watson et al. 2019).

To determine the effect of contamination on the main conclusions of this Letter, we generated 100 sets of the four samples (EELGs, control, mass-matched, and mass plus sSFR–matched control) by randomly removing 30% of the companions identified for each galaxy. For each iteration and sample, we calculated the median number of companions, the mass
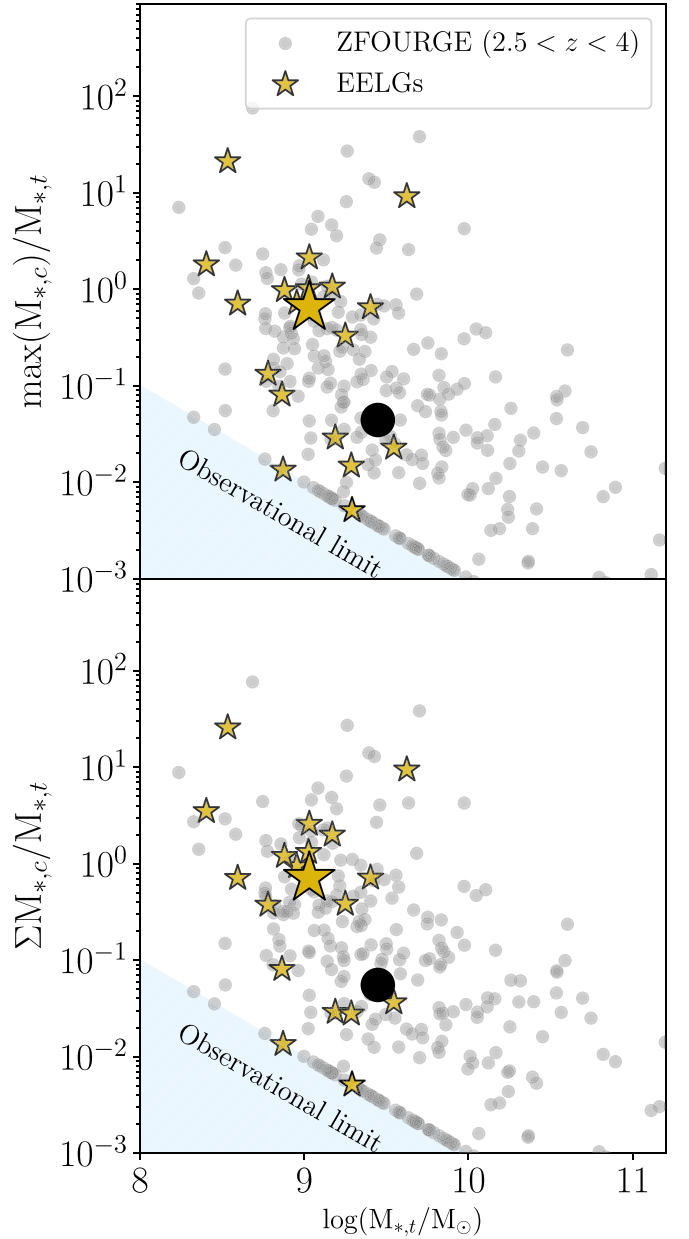
Figure 4. The ratio of stellar mass of the brightest companion (top) and total stellar mass of all companions (bottom) to the target galaxy as a function of stellar mass of primary targets. Color scheme is the same as Figure 1. The larger symbols represent the median of the respective samples. The blue shaded region represents the stellar mass limit ($\log(M_*/M_\odot) = 7$) of our companion population. A higher stellar mass ratio of companions around EELGs suggests EELGs might be undergoing strong interaction/major mergers.

ratio of the brightest companion, and the total mass of all companions. We found very little overlap between the distributions of medians across all samples and parameters (KS test $p < 0.001$).

The median number of companions for EELGs remained one, whereas for the full control sample, after removing 30% of companions, the median number became zero in all iterations. Similarly for the stellar mass- and stellar mass plus sSFR–matched control samples, the median number of companions became zero in about 50% of the iterations. The median mass ratio of the brightest companion [the median ratio of the total stellar mass of all companions] was $0.13^{+0.01}_{-0.07}$ [$0.22^{+0.02}_{-0.16}$], $0.03^{+0.02}_{-0.01}$ [$0.03^{+0.03}_{-0.01}$], $0.03^{+0.03}_{-0.01}$ [$0.03^{+0.04}_{-0.01}$], and $0.008^{+0.001}_{-0.001}$
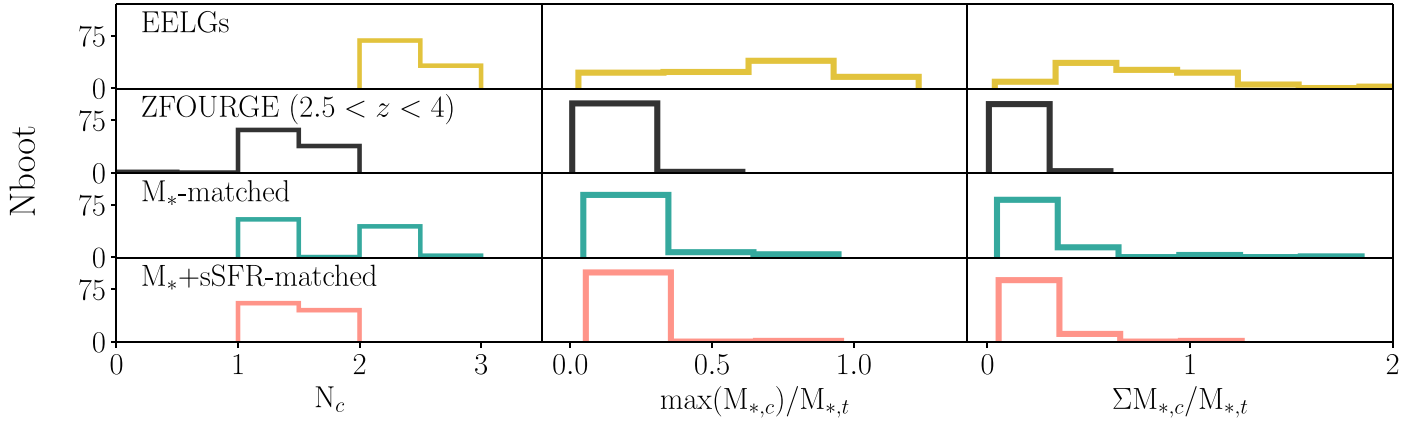
Figure 5. Bootstrapped distribution of the median number of companions (left), the stellar mass ratio of the brightest companion (middle), and the total stellar mass ratio of all companions (right) for EELGs (top row), full control sample (second row), stellar mass–matched sample (third row), and stellar mass plus sSFR–matched sample (fourth row). EELGs have roughly similar stellar mass companion galaxies, whereas the stellar mass ratio of companions for all control samples is 3–10 times smaller.

$[0.008^{+0}_{-0.001}]$ for EELGs, mass-matched, mass plus sSFR–matched, and full control samples, respectively. After removing 30% of companions, EELGs still have almost 3 [6] times higher mass ratio of the brightest companion [total stellar mass of all companions] than the stellar mass and stellar mass plus sSFR–matched control sample. Therefore, assuming a 30% false companion contamination in our sample does not change the main conclusion of this Letter.

3.5. Test with TNG100 Simulations

To test the robustness of our companion identification technique, we use the TNG100 simulation, which is part of the IllustrisTNG suit of cosmological simulations (Marinacci et al. 2018; Naiman et al. 2018; Nelson et al. 2018; Pillepich et al. 2018; Springel et al. 2018). From TNG100, we select all galaxies with stellar and dark matter mass $>10^8 M_\odot$ at snapshot 25, i.e., $z = 3$.

We use the projected distance along the xy-axis and velocity separation along the z-axis to identify companions around each galaxy. At $d_{xy} < 40$ kpc, $|dv_z| < 10000$ km s^{-1} 72% of the galaxies have more than one companion, and for 61% of the galaxies all identified companions live in the same halo as the target galaxy. If we restrict d_{xy} to 20 kpc then only 19% of the galaxies have more than one companion, and for 85% of galaxies all companions live in the same halo as the target galaxy. At $d_{xy} < 60$ kpc all galaxies have more than one companion, but only 29% of galaxies' companions share the same halo as the target galaxy. The velocity separation only affects these measurements at $|dv_z| < 200$ km s^{-1} ($\sim 0.03\sigma_{NMAD}$ companion), which is not practical for observations given the uncertainty in photometric redshifts.

We use the merger history trees (Rodriguez-Gomez et al. 2015) to estimate the fraction of companions with same descendent as the target galaxy. At $d_{xy} = 40$ kpc, $|dv_z| < 10000$ km s^{-1}; for about 63% of galaxies all identified companions will merge into a common descendent. Also, for 99.8% of galaxies at least one companion has the common descendent as the target galaxy. Our measurements are similar to Snyder et al. (2017), who used a similar photometric redshift and projected distance approach on mock surveys with simulated data to find about 80% of galaxy pairs identified at $z = 2$ will merge by $z = 0$. This suggests that the projected phase-space approach used in this work can successfully identify galaxies that eventually merge together and might already be experiencing strong interactions.

4. Discussion and Conclusion

This Letter utilizes deep JWST/NIRCam photometry and accurate photometric redshifts from the JADES survey to demonstrate that major mergers and/or strong interactions may be driving the extreme emission lines. We analyze the properties of companion galaxies (projected distance <40 kpc, velocity separation of <10,000 km s^{-1}) around 19 EELGs and 275 control galaxies at redshifts $2.5 < z < 4$. Tests conducted using the TNG100 simulation confirm that nearly all galaxies will eventually merge with at least one companion galaxy by $z = 0$ (Section 3.5), affirming the robustness of our companion identification technique.

We find that the median mass ratio of the most massive companion and the total mass ratio of all companions around EELGs are $0.65^{+0.11}_{-0.51}$ and $0.71^{+0.27}_{-0.34}$, respectively. In contrast, for control galaxies at similar redshifts these ratios are only $0.05^{+0.05}_{-0.02}$ (KS test $p = 0.007$) and $0.07^{+0.04}_{-0.04}$ ($p = 0.006$). Even after comparing with a stellar mass– and stellar mass plus sSFR–matched control sample, EELGs have 3 to 5 times higher mass ratios of the brightest companion and total mass of all companions (Figure 5). Our measurements suggest that EELGs are more likely to be surrounded by relatively more massive companion galaxies. We need spectroscopic data to confirm whether galaxies are undergoing major mergers or just experiencing strong interactions.

Mergers and galaxy–galaxy interactions can induce the circumgalactic medium gas to cool down and boost the star formation rate by 30%–40% as shown by detailed hydro-dynamical simulations (Moreno et al. 2019; Sparre et al. 2022). Some studies find evidence of bursty/rising star formation histories in EELGs (Cohn et al. 2018; Endsley et al. 2023). We find that companions around EELGs are relatively more massive even compared to the stellar mass plus sSFR–matched sample. This suggests that extreme emission lines might be produced at a significantly shorter timescale than the typical timescale of SFRs estimated from the SED models (~ 100 Myr). We suspect that gas cooling induced by strong interactions/mergers could be triggering the starburst episodes, which, in turn, produces the extreme emission lines.

Cosmological simulations predict an almost two-order increase in the merger rate between $z = 0$ and 6 (Hopkins et al. 2010; Rodriguez-Gomez et al. 2015). Deep photometric investigations have also confirmed the monotonic increase in the merger rate until $z = 6$ (Duncan et al. 2019). We hypothesize that the increased merger rate might be responsible for the overabundance of EELGs detected with JWST at $z > 6$ (Cameron et al. 2023; Endsley et al. 2023; Rinaldi et al. 2023; Tang et al. 2023). Thus, properly accounting for mergers would be important while estimating physical properties of gas and stars, in particular their kinematics and morphology in the early Universe.

Acknowledgments

Appendix

Table 2 presents the list of EELGs located within the JADES DR1 footprint, along with properties of companion galaxies identified around each EELG, as determined by the criteria outlined in Section 3.3.

Table 2
EELGs and Properties of Their Companions Galaxies

ZFOURGE ID	R.A. (J2000)	Decl. (J2000)	z	N_c	$\max(M_{*,c})/M_{*,t}$ [c]	$\Sigma M_{*,c}/M_{*,t}$ [d]
12533	53.1426	−27.8266	3.568[a]	3.0	9.19	9.43
12903	53.1795	−27.8239	3.17[b]	4.0	21.2	25.7
17189	53.1983	−27.7892	3.55[a]	3.0	1.81	3.49
17342	53.1434	−27.7881	3.41[b]	0.0	0.0135	0.0135
18742	53.1596	−27.7768	3.436[a]	4.0	0.133	0.374
11398	53.1533	−27.836	3.56[b]	1.0	0.708	0.708
11548	53.165	−27.8339	3.11[b]	2.0	0.722	0.939
15357	53.1408	−27.8041	2.616[a]	0.0	0.00512	0.00512
17583	53.1808	−27.7863	2.69[a]	2.0	1.02	1.32
18053	53.1958	−27.7828	3.326[a]	1.0	0.0806	0.0806
19656	53.2034	−27.7704	2.71[b]	2.0	0.649	0.714
19863	53.17	−27.7684	3.087[a]	1.0	0.029	0.029
20257	53.165	−27.7652	3.192[a]	2.0	0.0228	0.0364
22136	53.1529	−27.7493	3.088[a]	5.0	1.06	2.0
22277	53.1493	−27.7487	2.524[a]	0.0	0.00511	0.00511
13155	53.1757	−27.8223	3.064[a]	3.0	0.977	1.2
13203	53.1535	−27.8215	3.563[a]	3.0	2.13	2.58
15111	53.1612	−27.8062	2.987[a]	2.0	0.0148	0.0278
16603	53.1313	−27.793	3.61[b]	3.0	0.33	0.382

Notes.
[a] Spectroscopic redshift from the JADES DR1 or MOSEL surveys.
[b] Photometric redshift from the JADES DR1.
[c] $\max(M_{*,c})/M_{*,t}$ is the stellar mass of the most massive companion to the target galaxy.
[d] $\Sigma M_{*,c}/M_{*,t}$ is the total stellar mass of all companions to the target galaxy.

ORCID iDs

Anshu Gupta ⓘ https://orcid.org/0000-0002-8984-3666
Ravi Jaiswar ⓘ https://orcid.org/0000-0003-2035-3850
Vicente Rodriguez-Gomez ⓘ https://orcid.org/0000-0002-9495-0079
Ben Forrest ⓘ https://orcid.org/0000-0001-6003-0541
Kim-Vy Tran ⓘ https://orcid.org/0000-0001-9208-2143
Themiya Nanayakkara ⓘ https://orcid.org/0000-0003-2804-0648
Anishya Harshan ⓘ https://orcid.org/0000-0001-9414-6382
Elisabete da Cunha ⓘ https://orcid.org/0000-0001-9759-4797
Glenn G. Kacprzak ⓘ https://orcid.org/0000-0003-1362-9302
Michaela Hirschmann ⓘ https://orcid.org/0000-0002-3301-3321

References

Atek, H., Siana, B., Scarlata, C., et al. 2011, ApJ, 743, 121
Barro, G., Pérez-González, P. G., Cava, A., et al. 2019, ApJS, 243, 22
Brammer, G. B., van Dokkum, P. G., & Coppi, P. 2008, ApJ, 686, 1503
Bruzual, G., & Charlot, S. 2003, MNRAS, 344, 1000
Bunker, A. J., Cameron, A. J., Curtis-Lake, E., et al. 2023, arXiv:2306.02467
Cameron, A. J., Saxena, A., Bunker, A. J., et al. 2023, A&A, 677, A115
Charlot, S., & Fall, S. M. 2000, ApJ, 539, 718
Chevallard, J., Charlot, S., Senchyna, P., et al. 2018, MNRAS, 479, 3264
Cohn, J. H., Leja, J., Tran, K.-V. H., et al. 2018, ApJ, 869, 141
Conselice, C. J. 2003, ApJS, 147, 1
da Cunha, E., Charlot, S., & Elbaz, D. 2008, MNRAS, 388, 1595
da Cunha, E., Walter, F., Smail, I. R., et al. 2015, ApJ, 806, 110
Dressler, A., Rieke, M., Eisenstein, D., et al. 2023, arXiv:2306.02469
Duncan, K., Conselice, C. J., Mundy, C., et al. 2019, ApJ, 876, 110
Eisenstein, D. J., Willott, C., Alberts, S., et al. 2023, arXiv:2306.02465
Endsley, R., Stark, D. P., Chevallard, J., & Charlot, S. 2020, MNRAS, 500, 5229
Endsley, R., Stark, D. P., Whitler, L., et al. 2023, arXiv:2306.05295
Forrest, B., Tran, K.-v. H., Broussard, A., et al. 2018, ApJ, 863, 131
Gupta, A., Tran, K.-V., Mendel, T., et al. 2022, MNRAS, 519, 980
Gupta, A., Tran, K.-V., Pillepich, A., et al. 2021, ApJ, 907, 95
Hainline, K. N., Johnson, B. D., Robertson, B., et al. 2023, arXiv:2306.02468
Hayward, C. C., Narayanan, D., Kereš, D., et al. 2013, MNRAS, 428, 2529
Hopkins, P. F., Bundy, K., Croton, D., et al. 2010, ApJ, 715, 202
Kaasinen, M., Bian, F., Groves, B., Kewley, L., & Gupta, A. 2016, MNRAS, 465, 3220
Labbé, I., Oesch, P. A., Bouwens, R. J., et al. 2013, ApJL, 777, L19
Lin, L., Koo, D. C., Willmer, C. N. A., et al. 2004, ApJL, 617, L9

López-Sanjuan, C., Cenarro, A. J., Varela, J., et al. 2015, A&A, 576, A53
Lotz, J. M., Primack, J., & Madau, P. 2004, AJ, 128, 163
Lumbreras-Calle, A., López-Sanjuan, C., Sobral, D., et al. 2022, A&A, 668, A60
Mainali, R., Stark, D. P., Tang, M., et al. 2019, MNRAS, 494, 719
Mantha, K. B., McIntosh, D. H., Brennan, R., et al. 2018, MNRAS, 475, 1549
Marinacci, F., Vogelsberger, M., Pakmor, R., et al. 2018, MNRAS, 480, 5113
Maseda, M. V., van der Wel, A., da Cunha, E., et al. 2013, ApJL, 778, L22
Maseda, M. V., Van Der Wel, A., Rix, H. W., et al. 2014, ApJ, 791, 17
Moreno, J., Torrey, P., Ellison, S. L., et al. 2019, MNRAS, 485, 1320
Naiman, J. P., Pillepich, A., Springel, V., et al. 2018, MNRAS, 477, 1206
Nanayakkara, T., Glazebrook, K., Kacprzak, G. G., et al. 2016, ApJ, 828, 21
Nelson, D., Pillepich, A., Springel, V., et al. 2018, MNRAS, 475, 624
Oesch, P. A., Brammer, G., Naidu, R. P., et al. 2023, MNRAS, 525, 2864
Patton, D. R., Carlberg, R. G., Marzke, R. O., et al. 2000, ApJ, 536, 153
Pillepich, A., Nelson, D., Hernquist, L., et al. 2018, MNRAS, 475, 648
Popesso, P., Concas, A., Cresci, G., et al. 2022, MNRAS, 519, 1526
Reddy, N. A., Shapley, A. E., Sanders, R. L., et al. 2018, ApJ, 869, 92
Rieke, M. & the JADES Collaboration 2023, ApJS, 269, 16
Rieke, M., Robertson, B., Tacchella, S., et al. 2023, Data from the JWST Advanced Deep Extragalactic Survey (JADES), STScI/MAST, doi:10.17909/8TDJ-8N28
Rinaldi, P., Caputi, K. I., Costantin, L., et al. 2023, ApJ, 952, 143
Roberts-Borsani, G. W., Bouwens, R. J., Oesch, P. A., et al. 2016, ApJ, 823, 143
Rodriguez-Gomez, V., Genel, S., Vogelsberger, M., et al. 2015, MNRAS, 449, 49
Rose, C., Kartaltepe, J. S., Snyder, G. F., et al. 2023, ApJ, 942, 54
Sanders, D. B., & Mirabel, I. F. 1996, ARA&A, 34, 749
Snyder, G. F., Lotz, J. M., Rodriguez-Gomez, V., et al. 2017, MNRAS, 468, 207
Sparre, M., Hayward, C. C., Feldmann, R., et al. 2017, MNRAS, 466, 88
Sparre, M., & Springel, V. 2017, MNRAS, 470, 3946
Sparre, M., Whittingham, J., Damle, M., et al. 2022, MNRAS, 509, 2720
Springel, V., Pakmor, R., Pillepich, A., et al. 2018, MNRAS, 475, 676
Straatman, C. M. S., Spitler, L. R., Quadri, R. F., et al. 2016, ApJ, 830, 51
Tacchella, S., Dekel, A., Carollo, C. M., et al. 2016, MNRAS, 457, 2790
Tacchella, S., Forbes, J. C., & Caplar, N. 2020, MNRAS, 497, 698
Tang, M., Stark, D. P., Chen, Z., et al. 2023, MNRAS, 526, 1657
Tang, M., Stark, D. P., Chevallard, J., & Charlot, S. 2019, MNRAS, 489, 2572
Torrey, P., Vogelsberger, M., Hernquist, L., et al. 2018, MNRAS: Letters, 477, L16
Tran, K.-V. H., Forrest, B., Alcorn, L. Y., et al. 2020, ApJ, 898, 45
van der Wel, A., Straughn, A. N., Rix, H.-W., et al. 2011, ApJ, 742, 111
Watson, C., Tran, K.-V., Tomczak, A., et al. 2019, ApJ, 874, 63
Williams, C. C., Tacchella, S., Maseda, M. V., et al. 2023, ApJS, 268, 64
Williams, C., Tacchella, S., & Maseda, M. 2023, Data from the JWST Extragalactic Medium-band Survey (JEMS), STScI/MAST, 10.17909/FSC4-DT61